J|A|C|S
ARTICLES

Published on Web 03/11/2009

The Nature of Radiative Transitions in O-Doped Boron Nitride Nanotubes

Gaoyang Gou,[†] Bicai Pan,*[,†,‡] and Lei Shi*[,†]

Hefei National Laboratory for Physical Science at Microscale and Department of Physics, University of Science and Technology of China, Hefei 230026, P.R. China

Received December 7, 2008; E-mail: bcpan@ustc.edu.cn; shil@ustc.edu.cn

Abstract: Recent measurements on cathodoluminescences spectra of natural and isotope-substituted boron nitride nanotubes (BNNTs) surprisingly suggest the existence of pronounced radiative transitions in BN tubes, which are possibly induced by the oxygen substitutional impurities of the samples. [Han, W. Q. et al. *Nano Lett.* **2008**, *8*, 491] However, the structural pattern of the O-doped BN tube is unknown, as a result, how does the substitutional impurity in BNNT contribute to the observed radiative transitions is still a puzzle. Using first-principle calculations, we predict a novel, stable O-doped BNNT configuration. Such a structure contains one B_3O_6 group, which is similar to the structural unit of boron oxide. Our calculations demonstrate that this type of O substitutional impurity can result in some donor-like gap states in the electronic structure and lead to the significant changes on the optical properties of BNNTs. The vibrational properties of the O-doped BNNT and boron oxide are also investigated. Our work elucidates the origins for experimental findings and provides a strong theoretical evidence on the existence of O substitutional impurity-induced radiative transitions in BNNT systems.

1. Introduction

Boron nitride nanotubes (BNNTs), which represent one important class of inorganic tubular nanomaterials, have attracted considerable research interest ever since their discovery.[1,2] Despite the structural similarities between BNNTs and carbon nanotubes (CNTs), there are essential differences between the two systems. Contrary to CNTs whose electronic properties are strongly structure dependent, BNNTs are semiconductors with the band gap width of about 5.5 eV, almost independent of tube chirality and morphology.[3] In addition, BNNTs are more chemically and thermally stable than their carbon analogues.[4,5] Therefore, the uniform and stable semiconducting properties of BNNTs could open promising opportunities for their application in nanophotonic devices, such as the ultraviolet (UV) light emitters, excitonic lasers, etc.

Because of the poor quality of BNNT samples,[6] experimental study on the optical properties of BNNTs are challenging, but recent experiments have made significant progress. Experiments of Watanabe et al.[7] on luminescence spectra of single crystalline hexagonal BN (h-BN) have confirmed that h-BN has a direct band gap of 5.971 eV and demonstrated the potential application of h-BN for compact UV laser devices ($\lambda = 215.0$ nm). At first, the optical properties of BNNTs were investigated by means of electron energy loss spectroscopy (EELS).[8,9] Later on, the optical transitions of single-walled BNNTs were directly measured by Lauret et al., using optical absorption spectroscopy.[10] Three adsorption peaks were observed at 4.45, 5.50, and 6.15 eV, where the latter two energy lines were attributed to the strongly bound excitons of BN tubes.[11,12] Further, in the time-resolved photoluminescence (PL) spectroscopic studies of multiwalled BNNTs carried out by Wu et al., a broad emission peak between 3.5 and 4.2 eV was observed.[13] Zhi et al. observed a strong luminescence peak around 3.3 eV, as well as a shoulder at 4.1 eV, in the cathodoluminescences (CL) spectra of BNNTs.[14] Evidently, these experimental measurements on luminescence spectra of BNNTs almost provide a common finding: the dominant luminescence peak in BNNTs is always observed as a broadband, far below the near-band gap excitonic optical response of h-BN. Such a low-energy optical band will greatly decrease the luminous efficiency for potential usage of BNNTs as UV light sources.

[†] Hefei National Laboratory for Physical Science at Microscale, University of Science and Technology of China.
[‡] Department of Physics, University of Science and Technology of China.

(1) Rubio, A.; Corkill, J. L.; Cohen, M. L. *Phys. Rev. B* **1994**, *49*, 5081.
(2) Chopra, N. G.; Luyken, R. J.; Cherrey, K.; Crespi, V. H.; Cohen, M. L.; Louie, S. G.; Zettl, A. *Science* **1995**, *269*, 966.
(3) Blase, X.; Rubio, A.; Louie, S. G.; Cohen, M. L. *Europhys. Lett.* **1994**, *28*, 335.
(4) Pouch, J. J.; Alterovitz, A. *Synthesis and Properties of Boron Nitride*, Trans. Tech. Publ.: Switzerland, 1990, Vols. 54−55.
(5) Chen, Y.; Zhou, J.; Campell, S. J.; Caer, G. L. *Appl. Phys. Lett.* **2004**, *84*, 2430.
(6) Golberg, D.; Bando, Y.; Tang, C. C.; Zhi, C. Y. *Adv. Mater.* **2007**, *19*, 2413.
(7) Watanabe, K.; Taniguchi, T.; Kanda, H. *Nat. Mater.* **2004**, *3*, 404.
(8) Fuentes, G. G.; Borowiak-Palen, E.; Pichler, T.; Liu, X.; Graff, A.; Behr, G.; Kalenczuk, R. J.; Knupfer, M.; Fink, J. *Phys. Rev. B* **2003**, *67*, 035429.
(9) Arenal, R.; Stéphan, O.; Kociak, M.; Taverna, D.; Loiseau, A.; Colliex, C. *Phys. Rev. Lett.* **2005**, *95*, 127601.
(10) Lauret, J. S.; Arenal, R.; Ducastelle, F.; Loiseau, A.; Cau, M.; Attal-Tretout, B.; Rosencher, E.; Goux-Capes, L. *Phys. Rev. Lett.* **2005**, *94*, 037405.
(11) Park, C. H.; Spataru, C. D.; Louie, S. G. *Phys. Rev. Lett.* **2006**, *96*, 126105.
(12) Wirtz, L.; Marini, A.; Rubio, A. *Phys. Rev. Lett.* **2006**, *96*, 126104.
(13) Wu, J.; Han, W. Q.; Walukiewicz, W.; Ager, J. W.; Shan, W.; Haller, E. E.; Zettl, A. *Nano Lett.* **2004**, *4*, 647.
(14) Zhi, C. Y.; Bando, Y.; Tang, C. C.; Golberg, D.; Xie, R. G.; Sekigushi, T. *Appl. Phys. Lett.* **2005**, *86*, 213110.

Recent work of Han et al.[15] set the first step toward a conclusive understanding of the low-energy optical bands in BNNTs. The authors carried out experimental studies on band gap and radiative transition properties of BNNTs using CL spectroscopy. The rich CL spectra between 3.0 and 4.2 eV, associated with radiative transitions through a phonon−electron coupling process, were observed in their measurements. On the basis of the measured infrared (IR) spectra, they identified the observed low-energy optical bands as radiative transitions induced by oxygen substitutional impurities of the samples. Although Han et al. also performed some theoretical simulations on the O-doped BNNT structures, the microscopic origins of the radiative transitions are still unclear. Therefore, it is necessary to present systematically theoretical analysis on the structural, optical, and vibrational properties of O-doped BNNTs, which will be useful as a guideline for the experimental characterization of BNNT systems.

In this work, in order to reveal the nature of radiative transitions in the BNNT samples, we predict a novel stable O-doped BNNT configuration. We find that the oxygen substitutional impurity in such a configuration can give rise to some pronounced adsorption peaks in the optical spectra of BNNTs, which are consistent with experimental spectroscopic results. Significantly, our calculated eigen frequencies for the related vibrational modes can well match the IR and Raman peak positions experimentally observed. Our work not only provides the theoretical understanding of the experimental findings of Han et al. but also suggests a possible mechanism for interpreting and understanding previous experimental results on optical spectra of BNNTs.

2. Models and Methods

The calculations have been performed using the SIESTA code, within the spin-polarized density functional theory. The generalized gradient approximation (GGA) in the form of Perdew−Burke−Ernzerhof (PBE)[19] is adopted for the exchange-correlation functional. The norm-conserving pseudopotentials generated using the Troullier−Martins scheme,[20] with atomic core and nonlocal components expressed in the fully separable form developed by Kleiman and Bylander,[21,22] are used to represent the valence electrons. Sankey finite-range pseudo-atomic orbitals (PAOs)[23] are utilized as the split-valence double-ζ plus polarization basis set (DZP) for the valence electrons of all atoms involved.

A perfect (10, 0) BN tube, which consists of three times of primary unit cell along the axial direction, is used as the prototype model for a pristine tube. Periodical boundary condition is imposed along the axial direction of BNNT, and a vacuum region (at least 10 Å) is assumed between the tubes in their lateral direction. The Monkhorst−Pack scheme is used to sample the Brillouin zone.[24] The conjugated gradient (CG) algorithm is employed for the structure relaxation. For the structural optimization, we set the equivalent plane wave cutoff energy to be 120 Ry, the convergence of the force on each atom to be less than 0.02 eV/Å, and a set of six special k points along the tube axis is used. For the static (optical and lattice vibrational properties) calculations, we increase the cutoff energy to be 150 Ry, the force tolerance is set to be 0.01 eV/Å, and the mesh of k space is increased to $1 \times 1 \times 12$.

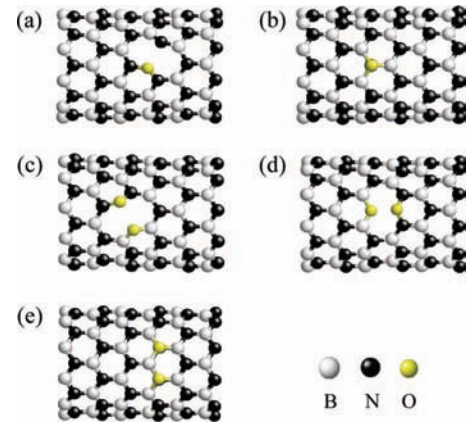

Figure 1. Geometric structures of O-doped (10, 0) BNNT for (a) O_B, (b) O_N, (c) O_{2t}, (d) O_{2a} and (e) BO_2 configurations. The distance between the two O atoms in O_{2t} and O_{2a} configurations is 2.467 and 2.304 Å, respectively. No bond is formed between the two O atoms.

3. Results and Discussion

3.1. Structural and Electronic Properties of O-Doped BNNT. Before generating the structural model, we notice that boron oxide (B_2O_3) is the most frequently used source of boron in the synthesis of BNNTs.[25] Typically, Han et al. synthesized the single-walled and multiwalled BNNTs using boron oxide as the reactant. Moreover, the IR spectra of boron oxide were used as the reference to identify the oxygen species in the BNNT samples.[15] It is therefore suggested that O contaminations in BNNTs may originate from the oxygen species of reactant boron oxide during the synthesis procedure.

In light of this finding, it is reasonable to assume that O species most probably act as a dopant in the BNNTs. In our calculations, the following O-doped BNNT configurations are considered first: replacing a single B or N atom with O (named as O_B or O_N), replacing a BN bond by an O−O dimer (the direction of the O−O dimer is either parallel or tilted to the tube axis, and the resulting configurations are denoted as O_{2a} and O_{2t} respectively), and substituting two nearest-neighboring N atoms (the resulting configuration exhibits BO_2N triangular structure, denoted as BO_2). The optimized structures for these configurations are displayed in a and b of Figure 1, where the structural features of O_B and O_N are well consistent with the O-doped BNNT model given by Han et al.[15]

The O-doped BNNT structures in Figure 1 are obtained by randomly substituting B or N atoms by O, without considering the experimental environment. Since oxygen dopant in BNNTs originates from the reactant boron oxide, a better understanding of boron oxide will be helpful for predicting the stable O-doped BNNT model.

Boron oxide is known as one of the most difficult compounds to crystallize, which is always found in the vitreous (amorphic) form. The structure of vitreous boron oxide has been studied by X-ray diffraction measurement.[26] As shown in Figure 2a,

(15) Han, W. Q.; Yu, H. G.; Zhi, C. Y.; Wang, J. B.; Liu, Z. X.; Sekiguchi, T.; Bando, Y. *Nano Lett* **2008**, *8*, 491.
(16) Ordejón, P.; Artacho, E.; Soler, J. M. *Phys. Rev. B* **1996**, *53*, R10441.
(17) Sánchez-Portal, D.; Ordejón, P.; Artacho, E.; Soler, J. M. *Int. J. Quantum Chem.* **1997**, *65*, 453.
(18) Soler, J. M.; Artacho, E.; Gale, J. D.; García, A.; Junquera, J.; Ordejón, P.; Sánchez-Portal, D. *J. Phys.: Condens. Matter* **2002**, *14*, 2745.
(19) Perdew, J. P.; Burke, K.; Ernzerhof, M. *Phys. Rev. Lett.* **1996**, *77*, 3865. *ibid*. **1997**, *78*, 1396.
(20) Troullier, N.; Martins, J. L. *Phys. Rev. B* **1991**, *43*, 1993.
(21) Kleinman, L.; Bylander, D. M. *Phys. Rev. Lett.* **1982**, *48*, 1425.
(22) Bylander, D. M.; Kleinman, L. *Phys. Rev. B* **1990**, *41*, 907.
(23) Sankey, O. F.; Niklewski, D. J. *Phys. Rev. B* **1989**, *40*, 3979.
(24) Monkhorst, H. J.; Pack, J. D. *Phys. Rev. B* **1976**, *13*, 5188.
(25) Arenal, R.; Stephan, O.; Cochon, J. L.; Loiseau, A. *J. Am. Chem. Soc.* **2007**, *129*, 16183.
(26) Mozzi, R. L.; Warren, B. E. *J. Appl. Crystallogr.* **1970**, *3*, 251.

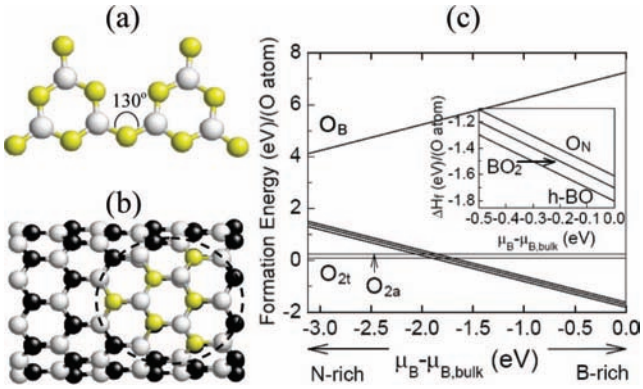

Figure 2. (a) Schematic diagram for the atomic structure in vitreous boron oxide. (b) Top view of the optimized structure for the h-BO O-doped (10, 0) BNNT configuration. The enlarged structure within the elliptical domain is shown in Figure 4d. (c) The calculated formation energy for each O-doped BNNT configuration, as a function of μ_B. The inset shows the formation energies of O_N, BO_2, and h-BO configurations under extreme B-rich environment. Note the formation energies are expressed in eV per O atom.

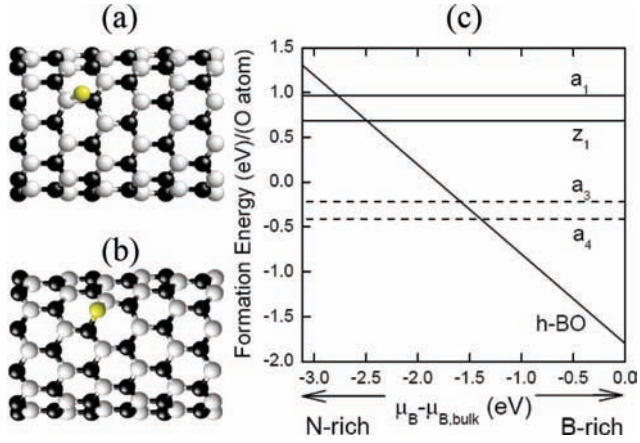

Figure 3. Fully optimized configurations with an O atom adsorbed at (a) axial and (b) zigzag bond sites of (10, 0) BNNT. (c) The formation energies for a_1, z_1, a_3 and a_4 O-adsorbed BNNT configurations, as well as h-BO O-doped configuration, as a function of μ_B. The formation energies of a_3 and a_4 (presented as dashed lines) configurations are taken from ref 28. Note the formation energies are expressed in eV per O atom.

the structural units of vitreous boron oxide are boroxol groups B_3O_6, which are composed of alternating 3-coordinated B and 2-coordinated O atoms. These groups are linked together by sharing the cornered O atoms, with randomness in the orientation about the B−O bond directions at the shared O atoms. The average B−O bond length is 1.37 Å. Within the hexagonal ring the average B−O−B angle is 120° and at the shared O it is approximately 130°.

The boroxol group B_3O_6 in vitreous boron oxide approximately characterizes the hexagonal structure, and the B−O bond length is close to the B−N bond length (1.44 Å in average) in BNNT. The structural similarity between the B_3O_6 group and the BN network indicates that oxygen species can smoothly incorporate BNNT structure by substituting six N atoms (three are within a hexagon, and the other three are directly bonding to it). In this way, the resulting O-doped BNNT configuration (contains one hexagonal B−O ring, abbreviated as h-BO configuration, displayed in Figure 2b) will bear the least structural deformation and possibly should be the most energetically preferable.

To evaluate the relative stability of the O-substituted configuration, its formation energy ΔH_f is calculated according to the following definition:[27]

$$\Delta H_f = E_{tot}[BON] - E_{tot}[\text{tube}] - n_B\mu_B - n_N\mu_N - n_O\mu_O \quad (1)$$

where E_{tot}[BON] is the calculated total energy of the O-doped BNNT, E_{tot}[tube] is the total energy of the reference system, a perfect (10, 0) BNNT. $n_{B(N,O)}$ (positive or negative) is the number of B(N,O) atoms being exchanged between the host tube and the atomic reservoir with chemical potential $\mu_{B(N,O)}$. Considering the equilibrium with BN tube, the μ_B (μ_N) is not independent but varies within the thermodynamically allowed range:

$$\mu_{B,bulk} + \Delta E_f[\text{tube}] < \mu_B < \mu_{B,bulk} \quad (2)$$

the upper limit corresponding to B-rich condition, with α-B phase used as the reservoir of μ_B; the lower limit refers to N-rich condition ($\mu_N = \mu_{N,N_2}$). The ΔE_f [tube] is the binding energy for a perfect (10, 0) BNNT (per B−N pair). Finally, μ_O is the free energy of O_2, which describes the abundance of O in the environment.

Figure 2c shows our calculated formation energies for each O-doped BNNT as a function of μ_B. Generally, O atoms are more favorable to substitute N from BNNT, as O_N, BO_2 and h-BO configurations have negative formation energies under extreme B-rich condition. Specifically, h-BO configuration is the most energetically favorable O-doped structure under B-rich condition. In the experiment, a liquid boron droplet is decomposed from boron compounds at first, BNNTs are then formed from the reaction between boron droplet and incoming N atoms.[25] It is indicated that the moderate B-rich condition is much closer to the experimental growth environment for BNNTs. Therefore, the h-BO configuration should be the most accessible O-doping impurity at the growth stage of BNNTs. The energetic preference of h-BO configuration is consistent with a priori assumption.

Without losing generality, we also extend our investigation to the cases where the as-grown BNNT products are contaminated by incoming O species, namely the oxygenation of BNNTs through surface adsorption.[28,29] We study the adsorption of a single O atom on (10, 0) BNNT first. Panels a and b of Figure 3 give the optimized configurations after one O atom is adsorbed at axial and zigzag bond site (named as a_1 and z_1, respectively). The formation energy ΔH_f is calculated according to formula 1, where E_{tot} [BON] refers to the energy of O-adsorbed BNNT and $n_{B,N} = 0$. Our calculated ΔH_f for a_1 and z_1 is 0.97 and 0.69 eV, respectively, well consistent with the reported results.[28] We find that ΔH_f remains positive even after the number of adsorbates on (10, 0) BNNT is increased to four. Xu et al.[28] reported that O atoms could adsorb on (5, 5) BNNTs exothermally, and the resulting configurations (such as a_3 and a_4) are quite stable. Comparing the formation energies between these O-adsorbed BNNT structures and the h-BO configuration (Figure 3c), it is found that the h-BO configuration is still energetically more favorable than O-adsorbed BNNTs under moderate B-rich condition.[30] Therefore, it is suggested that the oxygen species experimentally detected in BNNTs should originate from the substituting O atoms rather than surface

(27) Zhang, S. B.; Northrup, J. E. *Phys. Rev. B* **1991**, *67*, 2339.
(28) Xu, X.; Kang, H. S. *Chem. Mater.* **2007**, *19*, 3767.
(29) An, W.; Wu, X. J.; Yang, J. L.; Zeng, X. C. *J. Phys. Chem. C* **2007**, *111*, 14105.

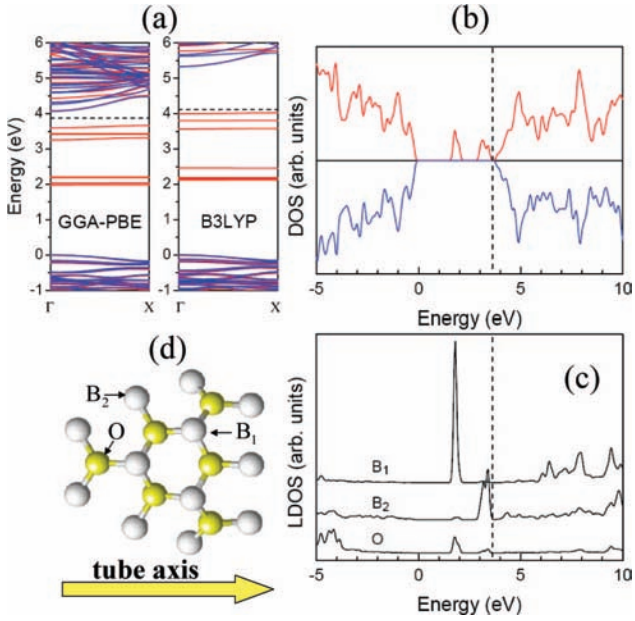

Figure 4. (a) Band structures of h-BO O-doped (10, 0) BNNT calculated using GGA-PBE and B3LYP functional. (b) Density of states (DOS) and (c) local density of states (LDOS) for the h-BO configuration calculated using GGA-PBE functional. (d) Local structure around the B_3O_6 group in the h-BO configuration. In (a) and (b), energy bands or DOS for the majority and minority spins are presented as red and blue lines, respectively. In (c), only LDOS for the majority spin is displayed. For better comparison, the energy levels of the valence band maximum (VBM) for the system are set at energy = zero. Fermi energy level (E_F) is presented as a dotted line.

adsorbate. Moreover, our h-BO O-substituting model is more convincing in explaining the X-ray photoelectron spectroscopy (XPS) results, that there are pronounced B−O bonding signals, but no N−O signals are found in BNNT samples synthesized by the thermal CVD method.[31]

Experimentally, a well-defined segregation between BN and C nanodomains has been probed in ternary BCN nanotubes.[32,33] It is natural to wonder whether the similar multiple domains also exist in O-doped BNNTs. In the hexagonal BCN network, the isoelectronic B−N and C−C bonds are much more stable than electron-deficient B−C and C−N bonds; henceforth, a separated C-BN domain structure is formed to minimize the unfavorable B−C or C−N bonds. However, if there do exist hexagonal BO domains in O-doped BNNTs (only B−O bonding signals are detected experimentally), the resulting B−O bond will be quite unstable, as the hexagonal BO structure is violating the electron counting rule. Typically, our calculated bond energy for a hexagonal B−O bond is 3.04 eV, much lower than that of a h-BN bond (3.97 eV). Therefore, the possibility for the formation of O-rich domains in O-doped BNNTs can be excluded.

In addition, the test calculations indicate that h-BO O-doping behavior for (12, 0), (5, 5) BNNT, and BN two-dimensional sheet is qualitatively the same as that for (10, 0) BNNT. Moreover, it is found that the h-BO configuration is also the most stable O-doped structure when varying the concentration of O dopant of BNNT. Thus, h-BO O-doped (10, 0) BNNT is an appropriate prototype model to simulate experimental results. In the following discussion, our investigation will focus on h-BO O-doped (10, 0) BNNT configuration only.

In h-BO configuration, the atomic structure of B_3O_6 group and the sp^2 bonding character of the BN network are all preserved, but it is worthy to note that, compared to the 2-coordinated O atoms in boron oxide, all the O atoms from B_3O_6 group in the h-BO configuration are triangularly surrounded by three B atoms. In other words, the extra geometrical constraint is imposed on the B_3O_6 group in the h-BO configuration. Such a change in the coordinating configuration may bring alteration to the physical properties of the system as well. To this end, the electronic structure of the h-BO configuration is under investigation.

The electronic structure of h-BO configuration is studied using the generalized gradient approximation in the form of Perdew−Burke−Ernzerhof (GGA-PBE) functional calculation at first. As shown in Figure 4, oxygen substitutional impurity induces the occupied impurity states in the gap region (majority spin channel) as a result of the extra valence electrons provided by O atoms. Significantly, comparing to the metallic O_N and BO_2 configurations with the partially occupied energy bands (Figures S1 and S2, Supporting Information), the semiconducting h-BO configuration is a more stable and more appropriate O-doped BNNT model.

A detailed analysis on the local density of states (LDOS) of the h-BO configuration reveals that impurity states lying around 2.0 eV are donated mainly by atoms from the B_3O_6 group, while the gap states around 3.5 eV are contributed from the B atoms bonding with B_3O_6 group. The donor-like states around 3.5 eV are also dispersed over the Brillouin zone in the band structure. Moreover, the h-BO O-doped BNNT is an indirect gap semiconductor with the bottom of the conduction band at the Γ point and the top of the impurity band at the *X* point. Therefore, it is expected that in the h-BO configuration the O substitutional doping will result in pronounced modification of the electronic and optical properties of BNNT systems.

However, a major concern with the above band structure discussion is the band gap error of the GGA functional calculation,[34,35] which is known to give unreliable energy levels for the gap states of O-doped BNNTs. The hybrid density functional approximation, such as B3LYP,[36,37] is commonly used as the alternative to GGA functional. B3LYP is the parametrized functional method that can provide reliable band gaps and defect levels arising from the impurities by employing the proper parameter. Therefore, in our calculation, the B3LYP method is employed to predict the band structure for h-BO O-doped BNNT (computational details can be found in the Supporting Information).

The band structures for the h-BO O-doped (10, 0) BNNT calculated using GGA-PBE and B3LYP functional are displayed in Figure 4a. It is found that, despite the significant corrections to the GGA band gap (increased by 1.2 eV), the relative energy

(30) According the definition of Formula (1), the formation energy of a given defect system will vary for different reference with different binding energy. Formation energies of a_3 a_4 are calculated using (5, 5) BNNT as the reference system. But the calculated binding energy difference (per B-N pair) between (5, 5) and (10, 0) BNNT is as small as 68 meV, which will not change the absolute formation energy of the corresponding system. Therefore, the formation energies for a_3 a_4 O-adsorbed (5, 5) BNNT and h-BO O-doped (10, 0) BNNT configurations are comparable.

(31) Kim, S. Y.; Park, J.; Choi, H. Y.; Ahn, J. P.; Hou, J. Q.; Kang, H. S. *J. Am. Chem. Soc.* **2007**, *129*, 1705.
(32) Enouz, S.; Stéphan, O.; Cochon, J.-L.; Colliex, C.; Loiseau, A. *Nano Lett.* **2007**, *7*, 1856.
(33) Enouz-Védrenne, S.; Stéphan, O.; Glerup, M.; Cochon, J.-L.; Colliex, C.; Loiseau, A. *J. Phys. Chem. C* **2008**, *112*, 16422.
(34) Hybertsen, M. S.; Louie, S. G. *Phys. Rev. Lett.* **1985**, *55*, 1418.
(35) Hybertsen, M. S.; Louie, S. G. *Phys. Rev. B* **1986**, *34*, 5390.
(36) Lee, C.; Yang, W.; Parr, R. G. *Phys. Rev. B* **1988**, *37*, 785.
(37) Becke, A. D. *J. Chem. Phys.* **1993**, *98*, 5648.

levels of gap states to the valence band maximum (VBM) change slightly in the B3LYP band structure. As a result, a rigid shift of 1.2 eV to the unoccupied conduction bands, namely scissor operator, can be added to correct the GGA band structure for the h-BO O-doped BNNT. Such a correction will be crucial to provide reliable spectroscopic results for O-doped BNNT systems using GGA functional calculation.

3.2. Optical and Lattice Vibrational Spectra. Han et al. observed a series of strong luminescence peaks within the energy region of 3.0−4.2 eV in their CL spectra of BNNT samples. On the basis of the measured IR spectra, it is suggested that these peaks could be induced by O-doped impurities in BNNTs. To simulate the spectroscopic results and provide theoretical understanding to the experimental findings, in this subsection, the optical and lattice vibrational properties of the h-BO configuration are under investigation.

The dielectric function and the electron energy-loss spectrum (EELS) are calculated to reveal the optical properties of BNNT systems. In our work, the optical properties are calculated on the basis of the dipolar transition approximation,[38] where the many-electrons effects i.e., excitonic effects, are neglected (Figure S3, Supporting Information). Theoretical calculations have indicated that the optical responses of BN tubes and h-BN should be dominated by strong excitonic effects. Typically, Park et al. predicted that the first excitonic peak of (8, 0) BNNT should be at 5.72 eV.[11] Moreover, it is demonstrated that the absolute position of the first excitonic peak in BNNT system is almost independent of the tube radius and system dimensionality.[12] It is therefore suggested that the exciton-related spectra exist at the near-band gap energy region, but for the low-energy luminescence peaks observed by Han et al., the excitonic effects can be neglected.[39] In this context, it is expected that the dipolar transition approximation could work well to predict the impurity-related adsorption spectra of O-doped BNNTs.

In the present calculation, dipolar transitions for both majority and minority spin channels of the h-BO configuration are taken into account. Because the optical anisotropy effects are not observed in CL spectra of BNNTs, in our work both longitudinal and transverse (light polarization parallel and perpendicular to the axis) optical excitation modes are included in the calculated dielectric function and EELS of BNNT. Moreover, the correction to the GGA band structure, namely a rigid shift of 1.2 eV to the conduction bands of the h-BO configuration, is introduced in optical properties calculation.

Figure 5 gives the calculated dielectric function and EELS for the h-BO configuration. For comparison, the imaginary parts of the dielectric function and EELS for a perfect (10, 0) BNNT are also presented. Compared to the perfect (10, 0) BNNT, the h-BO O-doped BNNT gives rise to a series of adsorption peaks (indicated by arrows in Figure 5) below the original band edge of the perfect (10, 0) BNNT. These peaks originate from the interband transitions between gap states and the conduction bands in the h-BO configuration (majority spin channel). For an indirect semiconductor, such as the h-BO O-doped BNNT, phonons must participate in the indirect electronic transition

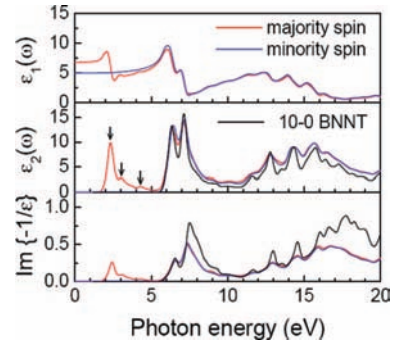

Figure 5. Calculated dielectric function and EELS for the h-BO configuration, where the majority spin and minority spin channels are represented as red and blue lines, respectively. ε_1 and ε_2 represent the real and imaginary parts of the dielectric function. Im$\{-1/\varepsilon\}$ refers to EELS. ε_2 and EELS of a perfect (10, 0) BNNT (black lines) are also plotted for comparison. The major peaks in the imaginary parts of dielectric function for h-BO configuration are indicated by arrows. A rigid shift to conduction bands by 1.2 eV is applied to obtain the results above.

process for the conservation of crystal momentum, which is a natural explanation of the rich phonon replica features observed in the luminescence spectra of the BNNT samples. Experimentally, the radiative transition peaks are identified at 4.092, 3.313, 3.081, and 2.679 eV. Our calculated peaks are at 4.279, 3.029, and 2.332 eV, very close to the experimental measurements. Therefore, it is concluded that there exist the strong radiative transitions induced by the oxygen substitutional impurity in the h-BO configuration, which is qualitatively consistent with the experimental findings.[40]

It is known that eigen frequency of the characteristic vibrational mode is an important physical quantity sensitive to the structural features of the system. In the work of Han et al., the characteristic B−O vibrational modes observed in the IR spectra of BNNT samples were served as the fingerprint for identification of oxygen species in BNNTs. Therefore, the theoretical simulation of phonon spectrum will be crucial for understanding of the experimental findings. In our work, the phonon spectrum is obtained by diagonalization of the dynamic matrix built by finite difference approximation (computational details are given in the Supporting Information). To compare the calculated phonon modes with experimental Raman and IR spectra, we restrict our discussion to first-order Raman or IR processes, where only phonons at (or close to) the Γ point of the Brillouin zone can be excited. In this way, the position of a given peak in Raman or IR spectra can be directly assigned to the calculated phonon frequency (at Γ point) of the corresponding mode.

Experimentally, the major Raman and IR peaks for the natural BNNTs were observed at 1366 and 1376 cm^{-1}, respectively.

(38) Madelung, O.; *Introduction to solid state theory*, edited by Cardona, M.; Fulde, P.; Queisser, H. J. (Springer-Verlag, New York, 1978).

(39) There are still posibilties that the low-energy peaks may arise from the excitons bound to impurity centers or dark excitons. We notice that the CL spectra of BNNTs were measured at room temperature. Under such a condition, excitons bound to impurities could be thermally dissociated and dark exciton related luminescence peaks would be very weak in intensity,[11] which are against the experimental findings.

(40) Simulation of photon emission spectra, such as CL spectra using first principle calculation is challenging. Based on experimental spectroscopic results, it is infered that radiative transitions in h-BO configuration should originate from the relaxation of the excited electrons from the conduction bands to the gap states. Therefore, the optical signals in the CL spectra will be close to the corresponding adsorption peaks in energy. Very recently, Lee *et al.*[41] successfully synthesized the multiwalled BNNTs samples using boric oxide CVD method (similar to synthetic techniques Han *et al.* used). A small adsorption peak at 3.7 eV was observed in their measured UV-visible absorption spectra. Under the similar growth condition, it is expected that h-BO O-doped impurity may also exist in BNNT samples of Lee *et al.*, which can give arise low-energy adsorption peak. Such an adsorption peak is very close to the luminescence peak of the CL spectra in energy, therefore further verifying our assumption.

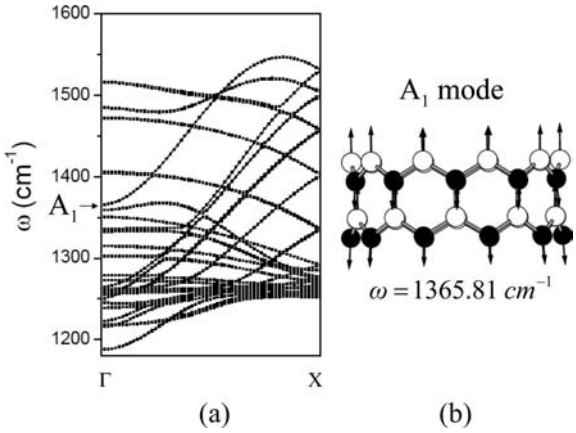

Figure 6. (a) Calculated phonon dispersion spectrum for the high-frequency modes of a (10, 0) BNNT. (b) The sketch of vibrational character for the high-frequency A_1 mode in a (10, 0) BNNT. Frequency (at Γ point) of the A_1 mode is also presented.

As illustrated by Han et al., these peaks can be ascribed to one intrinsic B−N vibration mode of BNNTs. If a zigzag BNNT is taken as a pristine model for BNNTs, its three A_1 and five E_1 vibrational modes are both Raman and IR active.[42] Moreover, Wirtz et al.[43] have predicted that the Raman intensity for the high-frequency A_1 mode (A_1 tangential mode) is the strongest of all modes for a zigzag BNNT, which was then proved by the experimental Raman spectroscopy of single-walled BNNTs.[44] Therefore, the B−N vibration signal of natural BNNTs detected by Han et al. can be assigned as the high-frequency A_1 mode. Our calculated frequency for such a phonon mode in (10, 0) BNNT is 1365.81 cm^{-1} (Figure 6), matching the experimental result very well.

The vibrational properties of boron oxide are also studied. As it is discussed in the first subsection, the atomic structure of vitreous boron oxide is noncrystalline. Therefore, an extremely large unit cell containing hundreds of atoms is needed to perform *ab initio* calculations for boron oxide, which will require a huge computational effort. To reveal the underlying vibrational features of boron oxide, a fictitious molecule has been taken as an alternative. As shown in the inset of Figure 7a, this fictitious molecule (named as "boroxol-hydride" molecule) is obtained from bonding three BH_2 groups to the cornered O atoms of one boroxol group. The optimized "boroxol-hydride" molecule characterizes C_{3h} symmetry. Determining from the geometric parameters of "boroxol-hydride" molecule (Table 1), it is found that the structural unit and the bonding characters of vitreous boron oxide are well preserved in the "boroxol-hydride" molecule. In this way, the structural properties of vitreous boron oxide are well reflected on the "boroxol-hydride" molecule. Therefore, under the simple-harmonic approximation, the main B−O vibrational features of boron oxide can be revealed from calculated vibrational modes of the B_3O_6 group in the "boroxol-hydride" molecule.

The calculated eigen frequencies for harmonic B−O vibrational modes in the "boroxol-hydride" molecule are displayed in Figure 7a. It is found that the matching between experimental IR peak position and calculated harmonic vibrational frequency[45] is surprisingly good. Only slight deviations are found at the low-frequency ($\omega < 700$ cm^{-1}) and high-frequency region ($\omega > 1400$ cm^{-1}).

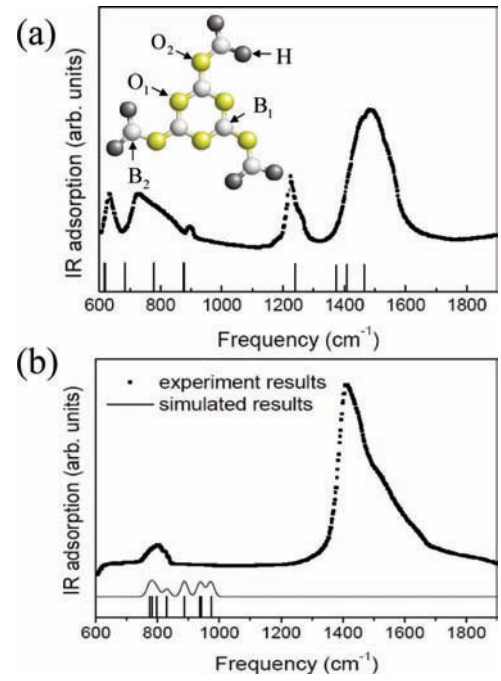

Figure 7. (a) Comparison between the experimental IR spectrum and the theoretical simulated vibrational modes for the boron oxide. The optimized structure of fictitious "boroxol-hydride" molecule is shown in the inset. (b) Experimental IR spectrum taken from the natural BNNTs, eigen frequencies and VDOS for B−O vibrational modes in the h-BO configuration. The harmonic vibrational frequency for each mode is indicated by a bar code. Experimental spectra are presented as dots, while theoretic simulations are shown as lines.

Table 1. Geometric Parameters for "Boroxol-Hydride" Molecule; Labels Used Are Shown in Figure 7a

	bond length (Å)		bond angle (deg)
B_1-O_1	1.385,1.386	$\angle O_1-B_1-O_1$	120.8
B_1-O_2	1.379	$\angle B_1-O_1-B_1$	119.2
B_2-O_2	1.376	$\angle O_1-B_1-O_2$	117.2, 122.0
B_2−H	1.234	$\angle B_1-O_2-B_2$	127.3

Experimentally, O-doped impurities in BNNTs could give rise to the characteristic B−O vibrational modes, which were detected in the IR spectra of BNNT samples. In order to reveal the B−O vibrational modes in the h-BO configuration, its vibrational frequencies and eigenvectors of the related modes are studied. The calculated phonon frequencies for the h-BO configuration are all positive, indicating the vibrational stability of the system. After carefully examining the eigenvectors of the calculated vibrational modes, we identify all characteristic B−O vibrational modes in the h-BO configuration. These modes have similar features: the atomic displacements with large amplitude are contributed from the atoms of the B_3O_6 group,

(41) Lee, C. H.; Wang, J.; Kayatsha, V. K.; Huang, J. Y.; Yap, Y. K. *Nanotechnology* **2008**, *19*, 455605.
(42) Wirtz, L.; Rubio, A.; Concha, R. A.; Loiseau, A. *Phys. Rev. B* **2003**, *68*, 045425.
(43) Wirtz, L.; Lazzeri, M.; Mauri, F.; Rubio, A. *Phys. Rev. B* **2005**, *71*, 241402.
(44) Arenal, R.; Ferrari, A. C.; Reich, S.; Wirtz, L.; Mevellec, J. Y.; Lefrant, S.; Rubio, A.; Loiseau, A. *Nano Lett.* **2006**, *6*, 1812.

(45) For a "boroxol-hydride" molecule with C_{3h} symmetry, The A' and E'' phonon modes are not IR active in principle. However, bulk boron oxide characterizes the lower symmetry (C_3 point group or $P3_1$ space group for h- B_2O_3), where both A and E modes are IR active. Considering the following transformation: A' A'' → A; E' E'' → E, all vibrational modes obtained in "boroxol-hydride" molecule should be IR active.

while the amplitude of vibrational eigenvectors for the other atoms are much smaller (Figure S4, Supporting Information). Thus, the characteristic B−O vibrational modes in the h-BO configuration are mainly localized at the B_3O_6 group, which can serve as the fingerprint for identification of O-doped impurities in BNNTs.

Figure 7b plots the calculated eigen frequencies and vibrational density of states (VDOS) for characteristic B−O vibrational modes in the h-BO configuration. A series of B−O vibrational modes spanning from 773 to 974 cm^{-1} are found. The experimental IR peak for the natural BNNTs centering at 800 cm^{-1} is within this region, and therefore can be assigned as B−O vibrational mode. However, the overlap peaked at 1460 cm^{-1} cannot be found in our simulations. We notice that this peak of natural BNNTs is quite close to one of the major peaks of boron oxide powder in frequency; thus, it is proposed that it might originate from boron oxide remnant of the samples. Moreover, the experimental observation that several IR peaks for B_2O_3 (at 634, 1196 cm^{-1}) are diminished from spectra of natural BNNTs is well reproduced in our simulations. This can be understood from the change of the coordinating configuration for B_3O_6 group. Compared to the B_3O_6 group in boron oxide, the extra geometrical constraint is imposed on B_3O_6 in the h-BO configuration. The change in the symmetry of the system makes some original vibrational modes incommensurate in the h-BO configuration, and therefore the corresponding IR peaks are diminished.

Our theoretical simulations on the h-BO O-doped BNNT configuration can account for the major experimental findings of Han et al.,[15] indicating the h-BO O-doped BNNT is a good theoretical model for understanding their results. It is noted that our simulation is performed on an isolated tube, whereas under the experimental conditions, the O-doping scenario in BNNTs will be quite complex due to the complicated environmental effects. Therefore, we cannot exclude the possibility of formation of other O-contaminated BNNT structures. However, considering the good match between the theoretical simulations and the experimental results, the h-BO O-doped BNNT configuration we proposed is still one of the most possible candidates, or at least serves as the basic pristine model for further experimental and theoretical investigation on such a system.

Very recently, Jaffrennou et al. performed CL and PL spectroscopy measurements on multiwalled BNNTs.[46] Their CL spectral features were quite similar to those of Han et al., with a dominant luminescence peak at the near-band gap region (233 nm) and an extra low-energy broadband around 320 nm (3.87 eV). Using the monochromatic CL image technique, the authors identified the broadband at 320 nm as an impurity-related luminescence band, which provided direct experimental evidence to our mechanism for understanding O substitutional impurity-induced radiative transitions.

The thermal CVD method has been extensively used for the synthesis of BNNTs,[47,48] and it is noticed that almost all BNNT samples used for optical characterizations were prepared using such a method. In the thermal CVD technique, volatile boron oxide vapors generated from the precursors are introduced to react with ammonia gas to form BNNTs. Because of the incomplete dissolution of the oxygen species,[25] O contamination will inhibit the reaction between boron and nitride species and therefore reside in the BN network. In this context, we propose that experimentally produced BNNT samples may inevitably contain more or less oxygen impurities and these impurities will lead to the low-energy optical bands commonly observed in luminescence spectra of BNNT systems.[13−15,46] Since the highly pure single crystalline h-BN samples have been successfully synthesized under a dry nitrogen atmosphere and the as-grown h-BN crystals were heat-treated at high temperature in N_2 to eliminate oxygen contaminations,[7] it is suggested that the similar synthetic method could be applied to produce high-quantity BNNT samples as well. Therefore, our prediction on the origins of low-energy optical bands of BNNTs can be tested by future luminescence results measured on oxygen-contamination-free BNNT samples.

4. Conclusions

In order to reveal the underlying nature for O substitutional doping-induced radiative transitions in BNNTs, we investigate the geometrical, optical, and vibrational properties of the O-doped BNNT systems by first-principles calculations. The stable O-doped BNNT structure is obtained by a replacement of some N atoms with O. On the basis of our calculations, the low-energy luminescence peaks experimentally observed can be identified as electronic transitions induced by the O substitutional impuriries of the system. Moreover, O-doped impurity of BNNT results in the characteristic B−O vibrational modes, which can serve as a fingerprint for experimental identification. Our theoretical simulations can account for major experimental findings of Han et al. and therefore illustrates the origins for their results. We also expect that our work may be helpful for understanding and interpreting several other spectroscopic results of BNNT samples.

Acknowledgment. J. Hu and Dr. W. T. Wu are acknowledged for their helpful discussions. This work is financially supported by the Ministry of Science and Technology of China (NKBRSF-G1999064603), National Basic Research Program of China (2006CB922000 and 2009CB939901), National Science Foundation of China (Grants 10874161 and 10574115), and the Innovation Foundation of USTC for the Postgraduate (KD2007079). The HP-LHPC of USTC is acknowledged for computational support.

Supporting Information Available: Electronic properties for all O-doped (10, 0) BNNT configurations under study; spin density distribution for the h-BO O-doped BNNT; computational details of B3LYP, optical and lattice vibrational properties calculations for h-BO configuration; vibrational features for characteristic B−O vibrational modes in the h-BO configuration. This material is available free of charge via the Internet at http://pubs.acs.org.

JA809550U

(46) Jaffrennou, P.; Barjon, J.; Schmid, T.; Museur, L.; Kanaev, A.; Lauret, J. S.; Zhi, C. Y.; Tang, C.; Bando, Y.; Golberg, D.; Attal-Tretout, B.; Ducastelle, F.; Loiseau, A. *Phys. Rev. B* **2008**, *77*, 235422.
(47) Tang, C.; Bando, Y.; Sato, T.; Kurashima, K. *Chem. Commun.* **2002**, 1290.
(48) Zhi, C.; Bando, Y.; Tang, C.; Golberg, D. *Solid State Commun.* **2005**, *135*, 67.